The use of a negative index planoconcave lens array for wide-viewing angle integral imaging

Hwi Kim, Joonku Hahn, and Byoungho Lee*

National Creative Research Center for Active Plasmonics Application Systems, Inter-University Semiconductor Research Center and School of Electrical Engineering, Seoul National University, Seoul 151-744, Korea
**Corresponding author: byoungho@snu.ac.kr*
http://oeqelab.snu.ac.kr

Abstract: Wide-viewing angle integral imaging by means of a negative refractive index planoconcave lens array is theoretically investigated. The optical properties of a negative refractive index lens are analyzed from the point of view of integral imaging. The effective focal length of a positive index planoconvex lens and a negative index planoconcave lens with the same surface spherical curvature R are approximated as $f_{P,eff} = 2R$ and $f_{N,eff} = 0.4R$, respectively. This short effective focal length of the negative index lens is advantageous for extending the viewing angle of the integral imaging. In addition, some other optical properties of a negative index lens are analyzed and compared for a positive index lens. Three-dimensional ray-tracing observation simulations of integral imaging systems with a negative index lens array and a positive index lens array are then performed, in a comparative study of the wide-viewing angle mode for integral imaging. A three-dimensional ray-tracing simulator for an integral imaging system is then developed. Some interesting issues that appear in the wide-viewing mode of integral imaging are discussed. The negative refractive index planoconcave lens was found to give a wider viewing angle of -60(deg.) ~ +60(deg.) and reduces aberration with only a single spherical planoconcave lens.

OCIS codes: (160.3918) Metamaterials, (080.0080) Geometric optics, (100.6890) Three-dimensional image processing.

References and links

1. B. Javidi and F. Okano, eds., *Three Dimensional Television, Video, and Display Technologies* (Springer, 2002).
2. B. Lee, J.-H. Park, and S.-W. Min, “Three-dimensional display and information processing based on integral imaging,” in *Digital Holography and Three-Dimensional Display*, T.-C. Poon, ed. (Springer, 2006), pp. 333-378.
3. H. Liao, M. Iwahara, H. Nobuhiko, and T. Dohi, “High-quality integral videography using a multiprojector,” Opt. Express **12**, 1067-1076 (2004).
4. X. Wang and H. Hua, “Theoretical analysis for integral imaging performance based on microscanning of a microlens array,” Opt. Lett. **33**, 449-451 (2008).
5. M. Kawakita, H. Sasaki, J. Arai, F. Okano, K. Suehiro, Y. Haino, M. Yoshimura, and M. Sato, “Geometric analysis of spatial distortion in projection-type integral imaging,” Opt. Lett. **33**, 684-686 (2008).
6. F. Okano, J. Arai, and M. Kawakita, “Wave optical analysis of integral method for three-dimensional images,” Opt. Lett. **32**, 364-366 (2007).
7. Y. Kim, J. Park, H. Choi, S. Jung, S. Min, and B. Lee, “Viewing-angle-enhanced integral imaging system using a curved lens array,” Opt. Express **12**, 421-429 (2004).
8. S. Jung, J.-H. Park, H. Choi, and B. Lee, “Viewing-angle-enhanced integral three-dimensional imaging along all directions without mechanical movement,” Opt. Express **11**, 1346-1356 (2003).
9. J. Jang and B. Javidi, “Three-dimensional integral imaging with electronically synthesized lenslet arrays,” Opt. Lett. **27**, 1767-1769 (2002).

#101915 - $15.00 USD Received 23 Sep 2008; revised 22 Nov 2008; accepted 11 Dec 2008; published 17 Dec 2008

10. J.-H. Park, S. Jung, H. Choi, and B. Lee, "Viewing-angle-enhanced integral imaging by elemental image resizing and elemental lens switching," Appl. Opt. **41**, 6875-6883 (2002).
11. J.-H. Park, Y. Kim, J. Kim, S. -W. Min, and B. Lee, "Three-dimensional display scheme based on integral imaging with three-dimensional information processing," Opt. Express **12**, 6020-6032 (2004).
12. S.-W. Min, J. Kim, and B. Lee, "Wide-viewing projection-type integral imaging system with an embossed screen," Opt. Lett. **29**, 2420-2422 (2004).
13. H. Choi, J.-H. Park, J. Hong, and B. Lee, "Depth-enhanced integral imaging with a stepped lens array or a composite lens array for three-dimensional display," The 16th Annual Meeting of the IEEE Lasers & Electro-Optics Society (LEOS 2003), Tucson, AZ, **2**, 730-731, Oct. 2003.
14. J. Jang and B. Javidi, "Large depth-of-focus time-multiplexed three-dimensional integral imaging by use of lenslets with nonuniform focal lengths and aperturesizes," Opt. Lett. **28**, 1924-1926 (2003).
15. D. R. Smith, W. Padilla, D. C. Vier, S. C. Nemat-Nasser, and S. Schultz, "A composite medium with simultaneously negative permeability and permittivity," Phys. Rev. Lett. **84**, 4184-4187 (2000).
16. R. A. Shelby, D. R. Smith, and S. Schultz, "Experimental verification of a negative index of refraction," Science **292**, 77-79 (2001).
17. D. Schurig and D. R. Smith, "Negative index lens aberrations," Phys. Rev. E **70**, 065601 (2004).
18. D. Schurig and D. R. Smith, "Free-space microwave focusing by a negative-index gradient lens," Appl. Phys. Lett. **88**, 081101 (2006).
19. C. G. Parazzoli, R. B. Greegor, J. A. Nielsen, M. A. Thompson, K. Li, A. M. Vetter, and M. H. Tanielian, "Performance of a negative index of refraction lens," Appl. Phys. Lett. **84**, 3232-3234 (2004).
20. P. Vodo, P. V. Parimi, W. T. Lu, and S. Sridhar, "Focusing by planoconcave lens using negative refraction," Appl. Phys. Lett. **86**, 201108 (2005).
21. K.-Y. Kim, "Photon tunneling in composite layers of negative- and positive-index media," Phys. Rev. E **70**, 047603 (2004).
22. H. M. Ozaktas, Z Zalevsky, and M. A. Kutay, *The Fractional Fourier Transform with Applications in Optics and Signal Processing*, (Wiley, New York, 2001).
23. J.-H. Park, S.-W. Min, S. Jung, and B. Lee, "Analysis of viewing parameters for two display methods based on integral photography," Appl. Opt. **40**, 5217-5232 (2001).
24. G. Dolling, M. Wegener, C. M. Soukoulis, and S. Linden, "Negative-index metamaterial at 780nm wavelength," Opt. Lett. **32**, 53-55 (2007).
25. G. Dolling, C. Enkrich, M. Wegener, C. M. Soukoulis, and S. Linden, "Simultaneous negative phase and group velocity of light in a metamaterial," Science **312**, 892-894 (2006).

1. Introduction

Integral imaging (InIm) is considered to be one of the more feasible technologies for displaying three-dimensional (3D) objects [1-3]. The InIm display uses a lens array to multiplex directional parallax views of a 3D target object into the two-dimensional (2D) image plane in the form of an elemental image and demultiplexes the elemental image into a full parallax 3D image of the target object without the need for an additional viewing apparatus such as polarization glasses.

One of the challenging problems in InIm is extending the viewing angle. In the high viewing angle mode of InIm, problems associated with image distortion and flipping occur. Some theoretical studies on these problems have been reported [4-6]. Various approaches for enhancing the viewing angle of InIm have been made. The curved lens array [7] widens the viewing angle, but the curve feature is disadvantageous because of its thickness. Viewing angle enhancement approaches using time multiplexing schemes [8-11] can also extend the viewing angle, but require additional loads as high speed polarization switching or a mechanical lens array moving apparatus. The critical problem for the time multiplex approach is the high-speed driving of liquid crystal display panels.

The conventional setup employs a lens array composed of a simple spherical singlet. To date, a few studies on the lens array itself such as a grouped lens system or a functional material lens have been reported. Studies of the lens array structure have also been reported. An embossed screen [12] and an aspherical inhomogeneous lens array [13, 14] were used in these studies, but they fail to provide a fundamental solution to the problem of viewing angle enhancement. Innovations and new ideas regarding lens array itself to enhance the viewing angle continue to be needed.

In this paper, we theoretically investigate wide-viewing angle InIm using a negative refractive index lens array. Advances associated with the negative index medium have led to

#101915 - $15.00 USD Received 23 Sep 2008; revised 22 Nov 2008; accepted 11 Dec 2008; published 17 Dec 2008

an explosion of research and has highlighted some interesting potentials for creating unprecedented optical functions. Although the practical realization of negative index media is currently limited to a very narrow frequency bandwidth and limited structures, previous and theoretical studies indicate that its potential applications are considerable [15-21]. The compactness, aberration compensation properties, and imaging characteristics, and evanescent field component enhancement are known to be advantageous optical properties of a negative index lens. Despite of the theoretical and practical complexity associated with the realization of negative index media in the broad wavelength range, the resulting macroscopic physical law of light refraction and total internal reflection on the negative index media can be described by no other than the Snell's law of refraction. Thus, it is possible to analyze the imaging characteristics of InIm with a negative index lens array as well as the optical properties of the negative index lens itself using only the Snell's law. Regarding InIm, the most important feature of the negative index lens is its short effective focal length. Using this unique property of the negative index lens, it becomes possible to construct wide-viewing angle InIm and study the imaging characteristics of the wide-viewing angle InIm by means of a negative index lens array.

In this paper, we expand out the meaning of the negative index lens to InIm and the imaging characteristics of wide-viewing angle InIm with a negative index lens array. In Sec. 2, the focusing properties of the negative index planoconcave lens are accounted for with a comparative analysis of the positive index planoconvex lens. In Sec. 3, imaging simulations of InIm with the negative index lens array, performed by a self-developed ray-tracing simulator, are described. The comparative analysis of an InIm-based negative index lens and a conventional positive index lens array InIm is presented. Concluding remarks are found in Sec. 4.

2. Focusing property of negative index planoconcave lens

In this section, the focusing properties of a negative index planoconcave lens (NIL) are analyzed and the results compared with those for a conventional positive index planoconvex lens (PIL). The focusing characteristics of a specific lens are prerequisites for a better understanding of the imaging characteristics and performance of InIm, when a specific lens array is used.

In Figs. 1(a) and 1(b), the structures and ray traces of NIL and PIL with spherical curvature R are illustrated, respectively.

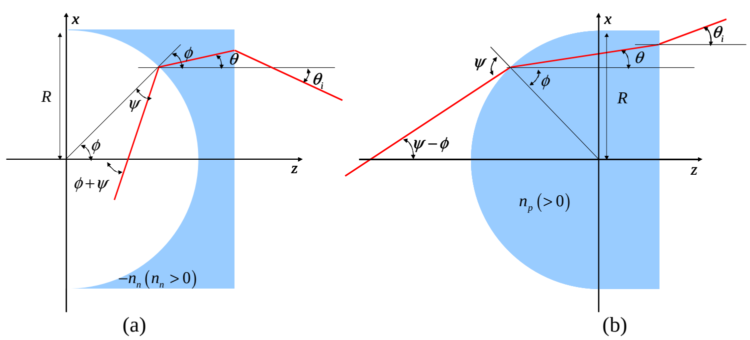

Fig. 1. Structures and ray traces of (a) negative index planocancave lens (NIL) and (b) positive index planoconvex lens (PIL).

For NIL, Snell's law at the incidence plane and at the spherical surface of the NIL is described, respectively, by

$$n_n \sin\theta = \sin\theta_i\,, \tag{1a}$$

$$n_n \sin(\phi-\theta) = \sin\psi\,, \tag{1b}$$

#101915 - $15.00 USD Received 23 Sep 2008; revised 22 Nov 2008; accepted 11 Dec 2008; published 17 Dec 2008

where θ_i and n_n are the incidence angle of a ray and the absolute value of the negative refractive index (Note that light rays are incident from the right in Fig. 1.). The refractive index of the surroundings is set to 1 (air). The ray trace in the left half-infinite air region is obtained by

$$x = R\sin\phi + (z - R\cos\phi)\tan(\psi + \phi). \tag{1c}$$

For PIL, Snell's law at the incidence plane and at the spherical surface of the PIL is described, respectively, by

$$n_p \sin\theta = \sin\theta_i, \tag{2a}$$

$$n_p \sin(\phi + \theta) = \sin\psi, \tag{2b}$$

where θ_i and n_p are the incidence angle of a ray and the positive refractive index. The ray trace in the left half-infinite air region is obtained by

$$x = R\sin\phi + (z + R\cos\phi)\tan(\psi - \phi). \tag{2c}$$

By default, let the lens curvature radius, R (taken as a positive value), the negative refractive index, $-n_n$, and the positive refractive index, n_p, be set to 1 (in the unit of coordinates), -1.5, and 1.5, respectively.

As shown in Figs. 1(a), 1(b), Eqs. (1c), and (2c), the crossing angle of the ray to the optic axis (*z*-axis) are $\psi + \phi$ and $\psi - \phi$ for NIL and PIL, respectively. With respect to the incidence position (z_i, x_i), the ray crossing angle varies. The parameter ϕ is given by a function of the incidence position (z_i, x_i), respectively, as

$$(z_i, x_i) = (R\cos\phi, R\sin\phi), \qquad \text{for NIL}, \tag{3a}$$

$$(z_i, x_i) = (-R\cos\phi, R\sin\phi), \qquad \text{for PIL}. \tag{3b}$$

The crossing angle is closely related to the effective focal length of the lens. In geometric optics, the focal length of a lens can be precisely defined for a paraxial region near the optic axis. Based on the lens maker's formula, the effective focal lengths for NIL and PIL in the paraxial region around the optic axis are obtained by $f_{N,eff} = 0.4R$ and $f_{P,eff} = 2R$, respectively. With the same spherical curvature, the focal length of NIL is five times shorter than that of PIL.

To estimate the focal point and spherical aberration for NIL and PIL, we determine the position of the crossing point position of the rays in the focal plane (*x*-axis). For an incidence point (z_i, x_i) in the incidence plane, the *x*-directional focus profiles, $x(x_i)$, of the NIL and the PIL at a fixed z_f are given, respectively, as, from Eqs. 1(c) and 2(c),

$$x(x_i) = R\sin\phi + (z_f - R\cos\phi)\tan(\psi + \phi), \qquad \text{for NIL}, \tag{4a}$$

$$x(x_i) = -R\sin\phi + (z_f - R\cos\phi)\tan(\psi - \phi), \qquad \text{for PIL}, \tag{4b}$$

where z_f is defined by the parameter that satisfies the minimization of the focus constraint defined as

$$flatness\left(x(x_i); -R \le x_i \le R, z = z_f\right) = \frac{\max\left(x(x_i)\right) - \min\left(x(x_i)\right)}{\max\left(x(x_i)\right) + \min\left(x(x_i)\right)}. \tag{5}$$

The meaning of the minimization of Eq. (5) is that the major portion of the rays that are incident on the incident on the incidence plane, $-R \le x_i \le R$, are maximally focused around a single focal point $x(x_i)$ at the optimal z_f, which is referred to as the effective focal plane. This definition of the effective focal plane is available for the entire range of incidence including non-paraxial incidence as well as the case of paraxial incidence case. The ray crossing point distribution with respect to the incidence position x_i is parameterized by the effective focal length. The focusing at the normal incidence condition is estimated. The minimum z_f is the effective focal plane of the lens. According to the numerical calculation, z_f for NIL and PIL at a normal incidence is obtained as, respectively, $z_f = 0.6$ and $z_f = -3$ in the geometries of Fig. 2, which is matched to the lens maker's formula. Figure 2 shows the ray tracing profiles of NIL and PIL at a normal incidence.

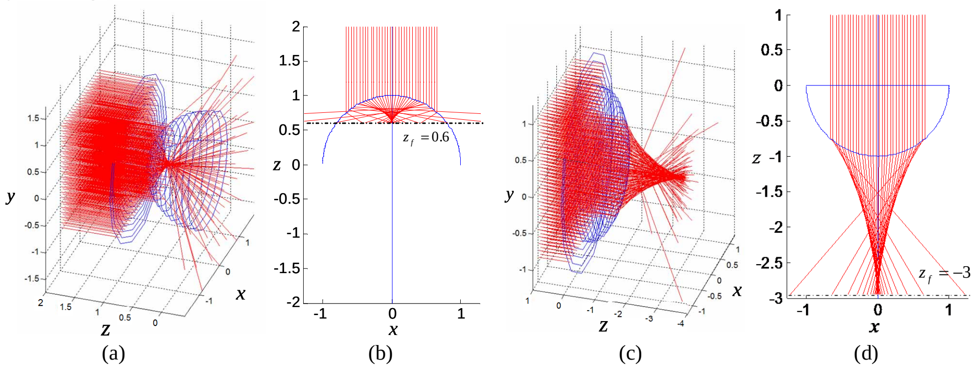

Fig. 2. Ray tracing profiles of NIL at normal incidence: (a) perspective view, (b) meridional cross-section, ray tracing profiles of PIL at normal incidence: (c) perspective view, (d) meridional cross-section.

On the other hand, in InIm, the spatial multiplexing of 3D images is obtained in the form of an elementary image. The elemental image is actually the image of the 3D target object captured by the same lens array. When displaying the elemental image through the lens array, spatial point image information distributed in the image plane is directionally displayed. A specific point information in the elemental image is brought along the corresponding directional ray through the corresponding elementary lens. Observers at different positions can visualize different parallax images. This Fourier transform property of the lens is the core of the InIm based 3D display system. The Fourier transform property of a lens is very important with respect to the applications to InIm systems. In Fig. 3, the Fourier transform properties of NIL and PIL for an incidence angle of $70(\text{deg.})$ are compared by ray-tracing. It should be noted that for an idence of $70(\text{deg.})$, the focal spot for NIL is formed within the range $-1 \le x \le 1$, while that for PIL is formed outside the range $-1 \le x \le 1$. In the case where the focal spot is formed like the PIL, flipping and image distortion are induced in InIm.

#101915 - $15.00 USD Received 23 Sep 2008; revised 22 Nov 2008; accepted 11 Dec 2008; published 17 Dec 2008

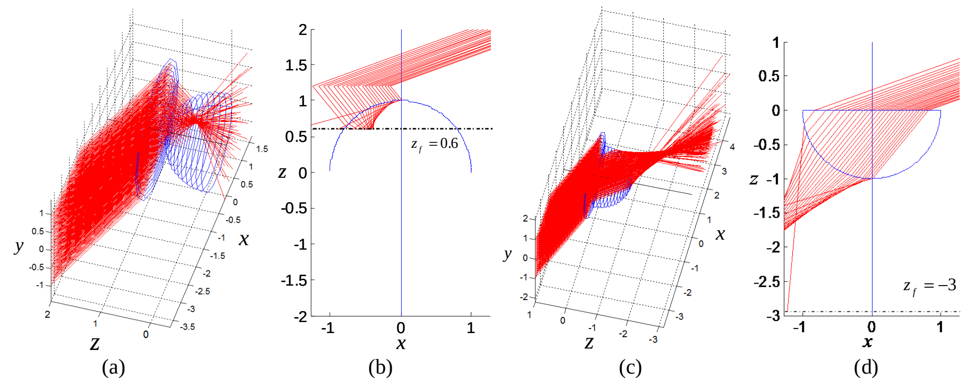

Fig. 3. Ray tracing profiles of NIL and PIL at oblique incidence of 70(deg.): (a) perspective view, (b) meridional cross-section of NIL and (c) perspective view, (d) meridional cross-section of PIL.

Figures 4(a) and 4(b) show the crossing point distributions $x(x_i)$ for the NIL (at $z_f = 0.6$) and the PIL (at $z_f = -3$) at normal incidence and an oblique incidence of $70(\text{deg.})$, respectively. In the normal incidence case, the crossing point distribution $x(x_i)$ assumes a symmetric form around $x_i = 0$. In an ideal case, all of the rays should be focused on $x(x_i) = 0$, which would be represented by a constant line $x(x_i) = 0$. However, for a practical spherical lens, the spatial deviation, i.e. aberration, with respect to the incidence position x_i is inevitable.

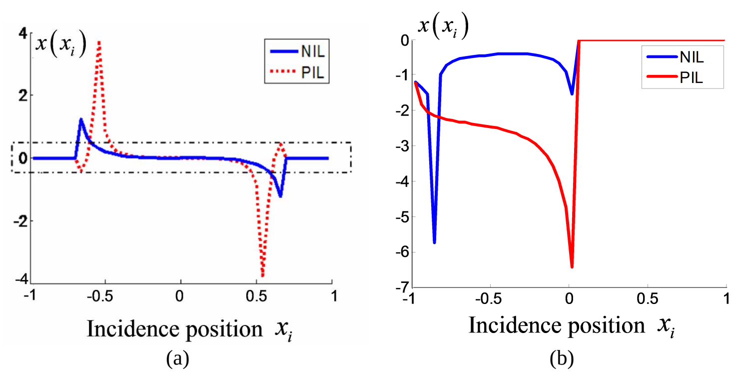

Fig. 4. Crossing point distribution, $x(x_i)$, for (a) normal incidence and (b) oblique incidence 70(deg.).

As can be seen in Fig. 4(a), the aberration level for PIL is no less than that for NIL. Near $x_i = \pm 1$, incident rays are totally internal-reflected and, as a result, do not contribute to the formation of the focus. In Fig. 4(b), the crossing point distribution $x(x_i)$ for an oblique incidence of 70(deg.) is shown. In this case, the PIL forms a highly aberrated focus, which is indicated by the inclined, non-flat $x(x_i)$ distribution (red lined). Meanwhile, the NIL forms a well-defined focus at $x = -0.5$, which is indicated by a relatively flat crossing point distribution (blue lined). In this oblique incidence case, the incident rays on $x_i > 0$ are totally internal-reflected for both cases of NIL and PIL. Let us look into, more carefully, the Fourier transform property and the transmission efficiency of NIL and PIL, as they are related to the

#101915 - $15.00 USD Received 23 Sep 2008; revised 22 Nov 2008; accepted 11 Dec 2008; published 17 Dec 2008

total internal reflection, more carefully. To accomplish this, let us define the spot width ρ and the spot position μ, for a specific continuous interval, $\left(x_{i,1}, x_{i,2}\right)$, in the incidence plane, respectively, as

$$\rho = \max\left(x\left(x_i\right)\right) - \min\left(x\left(x_i\right)\right) \qquad \text{for } x_i \in \left(x_{i,1}, x_{i,2}\right), \tag{6a}$$

$$\mu = \left[\max\left(x\left(x_i\right)\right) + \min\left(x\left(x_i\right)\right)\right]/2\,. \tag{6b}$$

The spot width physically defines the width of the area where all rays incident on the interval $\left(x_{i,1}, x_{i,2}\right)$ impinge at the focal plane. The spot position is the center of the area. Inversely, for a fixed spot width ρ, we can define the effective transmission window of a lens by the continuous interval $\left(\overline{x}_{i,1}, \overline{x}_{i,2}\right)$ in the incidence plane, such that the interval length, $w\left(\theta_i\right) = \left|\overline{x}_{i,2} - \overline{x}_{i,1}\right|$, is maximal as $w\left(\theta_i\right) = \left|\overline{x}_{i,2} - \overline{x}_{i,1}\right| = \max\left|x_{i,2} - x_{i,1}\right|$, where the effective transmission window varies with the incidence angle θ_i and so $w\left(\theta_i\right)$ is parameterized by the incidence angle θ_i.

In InIm, a point source is placed at a position in the focal plane under the lens. The rays that radiate from this point source are collimated to form a plane wave bundle that passes along a specific direction and the radiation is limited by the effective transmission window. The brightness of the pixel in InIm toward the viewing angle θ_i is determined by the effective transmission window. From the point of view of InIm, the parameter ρ is a measure of the degree of collimation. In Figs. 5(a) and 5(b), the focus position $\mu\left(\theta_i\right)$ and effective window $w\left(\theta_i\right)$ for various incidence angles for NIL, obtained by ray-tracing analysis, are shown as a function of $\sin\theta_i$, respectively. For comparison, in Figs. 5(c) and 5(d), the focus position $\mu\left(\theta_i\right)$ and the effective window $w\left(\theta_i\right)$ for various incidence angles for PIL are shown, respectively. In this simulation, the spot width ρ is set to 0.1. The spot position and the effective transmission window are defined for a specific incidence angle.

In the analysis of Fig. 5, it is possible to extract the effective focal lengths for NIL and PIL, which are the derivative, $-\partial\mu\left(\theta_i\right)/\partial\left(\sin\theta_i\right)$. In the paraxial region ($\left|\sin\theta_i\right| \le 0.5$), the linear relationship between the transverse vector of the incidence ray bundle, $\sin\theta_i$, and the transversal shift of the focal point from the center, $\mu\left(\theta_i\right)$ is confirmed. In the plot, the effective focal length f_{eff} is defined as

$$\mu\left(\theta_i\right) = f_{eff}\sin\theta_i\,. \tag{7}$$

In the cases of NIL and PIL, the effective focal length can be extracted, from the plots shown in Fig. 5, as, respectively,

$$f_{N,eff} = 0.4R\,, \tag{8a}$$

$$f_{P,eff} = 2R\,. \tag{8b}$$

This is in good agreement with results from the lens maker's formula. However, outside the paraxial region ($\left|\sin\theta_i\right| > 0.5$), the effective focal length f_{eff} is slightly larger than that of the

#101915 - $15.00 USD Received 23 Sep 2008; revised 22 Nov 2008; accepted 11 Dec 2008; published 17 Dec 2008

paraxial region and non-constant for both NIL and PIL. This focal length elongation can be attributed to image distortion associated with InIm, as demonstrated in the next section, which provides simulation data.

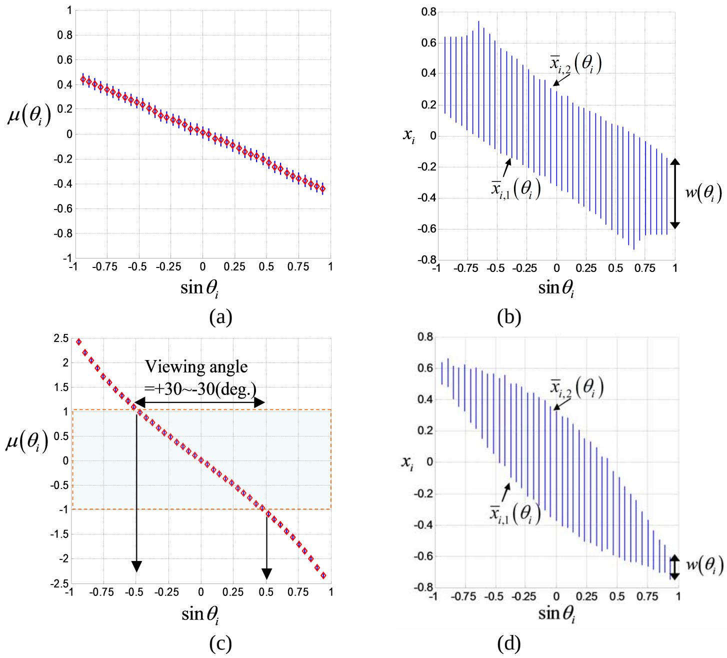

Fig. 5. Fourier transform properties of NIL and PIL: (a) focus position $\mu(\theta_i)$, (b) effective window $w(\theta_i)$ for NIL, and (c) focus position $\mu(\theta_i)$, (d) effective window $w(\theta_i)$ for PIL.

3. Simulation of integral imaging with negative index lens array

In this section, the effect and meaning of using an NIL array in InIm are discussed with self-developed 3D ray-tracing simulations. In particular, the imaging characteristics of wide-viewing InIm with the use of a NIL array are of main concern. For a comparative study, the InIm simulations with a perfect paraxial lens array and a PIL array are performed simultaneously.

A perfect paraxial lens is defined as a mathematical lens with zero-thickness, no-aberration, and a focal length of f. The key function of the perfect paraxial lens lies in its Fourier transform property such that an obliquely incident plane wave with an incidence angle of θ is focused at the position shifted by $f\sin\theta$ from the center in the focal plane. As shown in Fig. 5, both NIL and PIL have approximately linear Fourier transform properties, similar to this, perfect paraxial lens. Thus, the perfect paraxial lens is the ideal realization of spherical lenses as NIL and PIL. A critical difference between a perfect paraxial lens and NIL and PIL is the effective window size. The perfect paraxial lens focuses all of the incidence plane waves into an exact focus with no aberration and, as a result, the effective widow is the entire lens aperture. The mathematical transform for the perfect paraxial lens is represented by the 4×4 matrix [22]

$$\begin{pmatrix} 1-l_2/f & 0 & \lambda(l_1+l_2)-\lambda l_1 l_2/f & 0 \\ 0 & 1-l_2/f & 0 & \lambda(l_1+l_2)-\lambda l_1 l_2/f \\ 1/(\lambda f) & 0 & 1-l_1/f & 0 \\ 0 & 1/(\lambda f) & 0 & 1-l_1/f \end{pmatrix}\begin{pmatrix} u \\ v \\ \rho_u \\ \rho_v \end{pmatrix}=\begin{pmatrix} x \\ y \\ \rho_x \\ \rho_y \end{pmatrix}, \tag{9}$$

#101915 - $15.00 USD Received 23 Sep 2008; revised 22 Nov 2008; accepted 11 Dec 2008; published 17 Dec 2008

where λ is the wavelength, l_1 and l_2 are the distances between the (u,v) plane and the lens plane and the lens plane and (x,y) plane, respectively. f is the focal length of the lens. (u,v) and (ρ_u,ρ_v) are the starting point and the spatial frequency vector of a ray. The ray impinges through the lens on the point (x,y) with a spatial frequency vector of (ρ_x,ρ_y).

The InIm system is illustrated in Fig. 6. In the simulation, the lens array is composed of 41×41 elementary lenses with $1\text{cm}\times1\text{cm}$ rectangular apertures and the target 3D object is three letters, S, N, U positioned at $(x,y,z)=(-2\text{cm},5\text{cm},6\text{cm})$, $(3\text{cm},0,1\text{cm})$, and $(8\text{cm},-5\text{cm},-4\text{cm})$, respectively, as shown in Fig. 6.

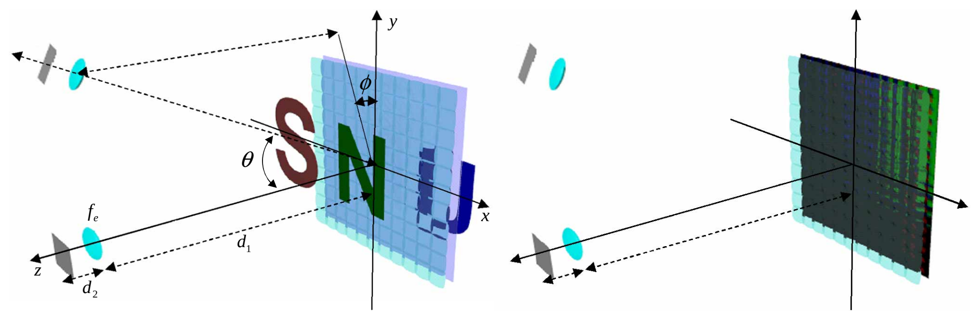

(a) (b)

Fig. 6. (a) pick-up setup and (b) display setup of InIm system.

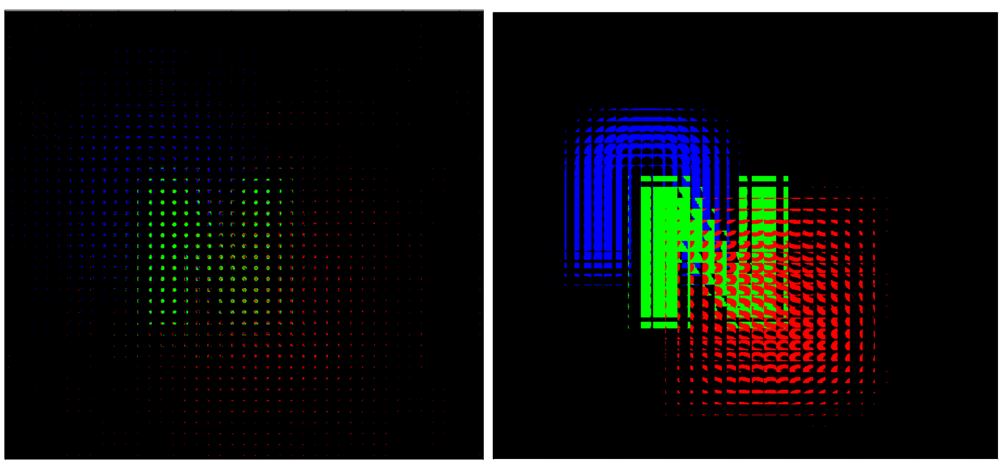

(a) (b)

Fig. 7. Elemental images (a) for NIL InIm with a lens focal length of $f_{N,eff}=0.2\text{cm}$ and (b) for PIL InIm with a lens focal length of $f_{P,eff}=1\text{cm}$.

InIm is capable of displaying both virtual and real objects when the gap between the lens array and elemental images is equal to the focal length of the lens. In the simulation setup, the letters S and N are the real objects and the letter U is a virtual object [23]. The observation camera is denoted by a simple perfect paraxial lens with a focal length of f_e. The center of the camera lens is placed at $(x,y,z)=(-d_1\sin\theta\sin\phi, d_1\sin\theta\cos\phi, d_1\cos\theta)$. The distance between the camera image plane and the camera lens is d_2. In the simulation, f_e, d_1, and d_2

#101915 - $15.00 USD Received 23 Sep 2008; revised 22 Nov 2008; accepted 11 Dec 2008; published 17 Dec 2008

are set to 4.97cm , 2m , and 5.1cm , respectively. The camera image plane is set to $12\text{mm}\times12\text{mm}$ that can capture the whole lens array.

The reverse projected image of the 3D scene through the lens array onto the 2D flat display panel as shown in Fig. 6(a) is referred to as the elemental image. The elementary image plane is placed on the focal plane of the lens array. The observer can then perceive the pixelate 3D image through the lens array in the display mode, as illustrated in Fig. 6(b). In this setup, the number of elemental lenses is the 3D image resolution. In the case of our simulation, the 3D image resolution is 41×41, the number of used elemental lenses used.

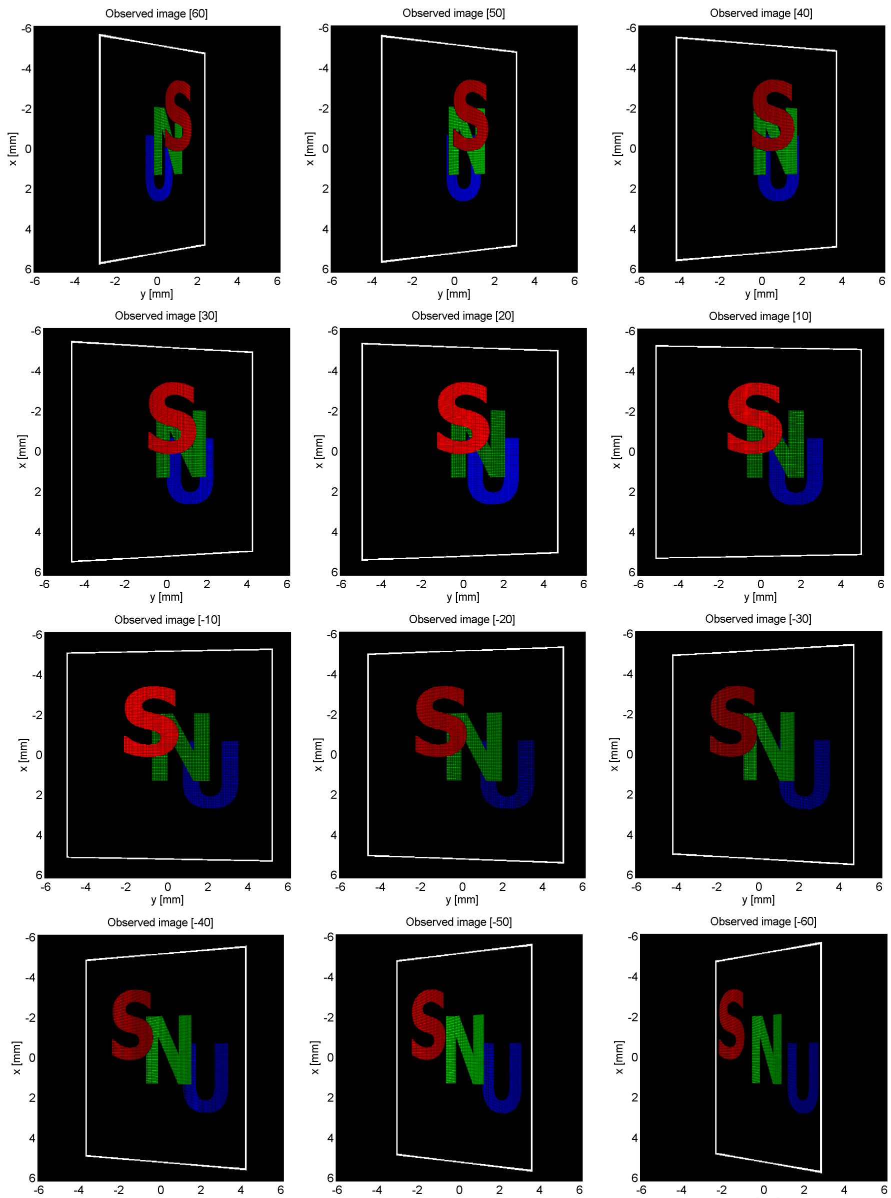

Fig. 8. Images of the 3D target object observed at various viewing angle position.

The synthesized elemental image may look quite different with respect to the lens focal length. In this paper, we examine the InIm systems with NIL with a focal length of

#101915 - $15.00 USD Received 23 Sep 2008; revised 22 Nov 2008; accepted 11 Dec 2008; published 17 Dec 2008

$f_{N,eff} = 0.4 \times 0.5\text{cm}=0.2\text{cm}$ and PIL with a focal length of $f_{P,eff} = 2 \times 0.5\text{cm}=1\text{cm}$. The elemental images for these NIL and PIL are presented in Fig. 7(a) and 7(b), respectively.

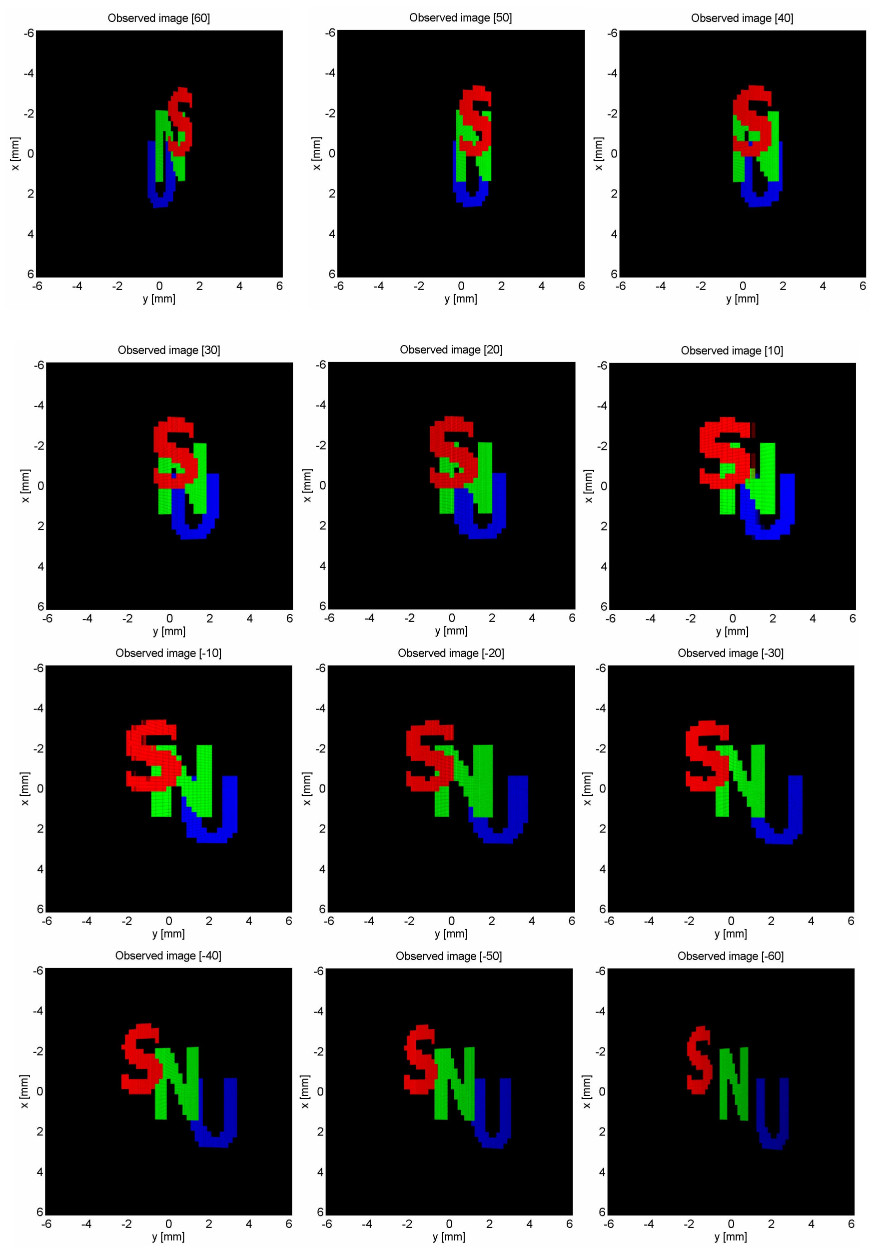

Fig. 9. Images of the InIm with paraxial perfect lens of focal length $f_{N,eff} = 0.2\text{cm}$.

In InIm, the synthesized 3D images are observed within the lens array domain. Because of this, the observation camera should capture the entire lens array and the observed image of the target 3D object should be within the boundary of the lens array. With this setup, the camera images of the 3D target object observed, when the viewing angle θ is varied from $+60(\text{deg.})$ to $-60(\text{deg.})$ and with ϕ fixed to $90(\text{deg.})$ are presented in Fig. 8.

#101915 - $15.00 USD Received 23 Sep 2008; revised 22 Nov 2008; accepted 11 Dec 2008; published 17 Dec 2008

The observation of the respective elemental images through the lens array is next performed at various viewing positions from $\theta = +60(\text{deg.})$ to $\theta = -60(\text{deg.})$. Three types of InIm using NIL, PIL and a perfect paraxial lens array are compared with each other and compared with observing the real object.

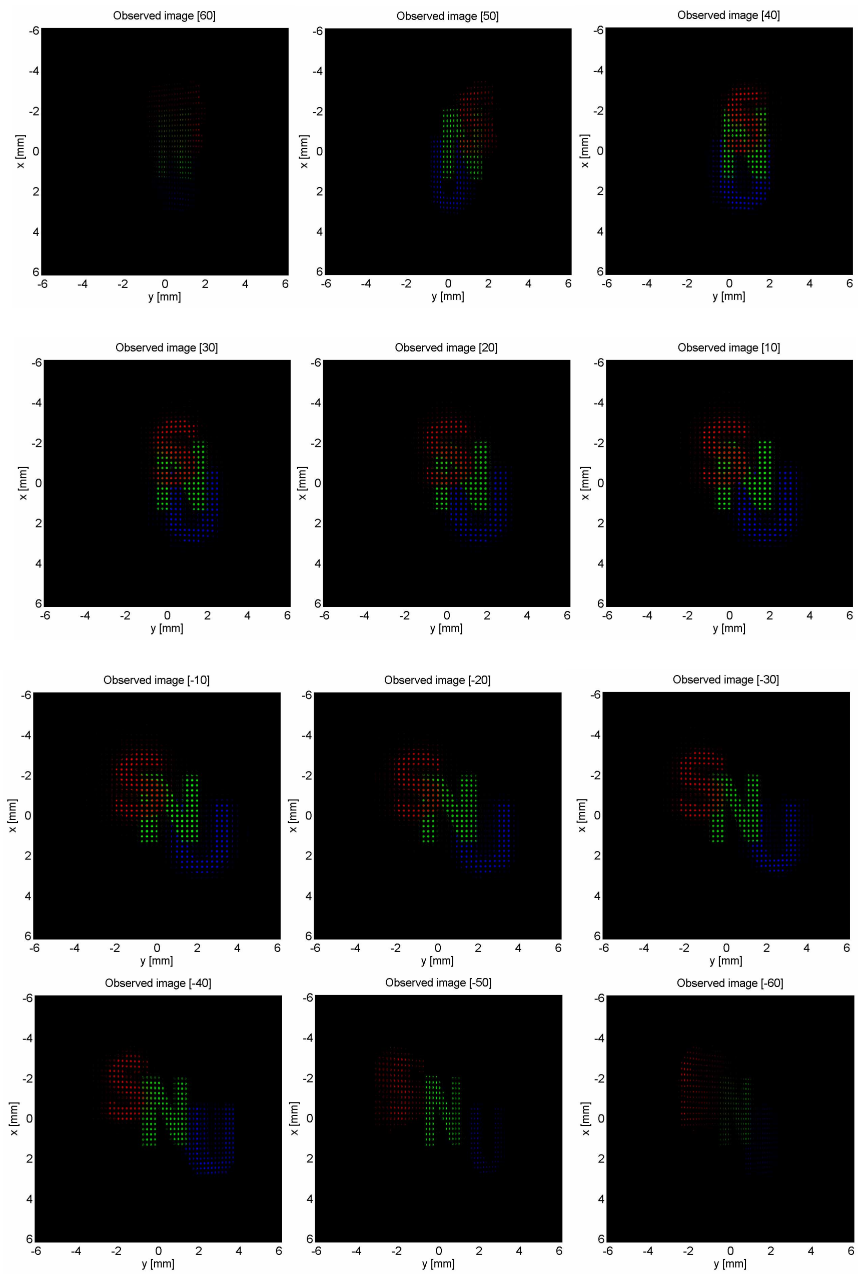

Fig. 10. Images of the InIm with an NIL array of effective focal length $f_{N,eff} = 0.2\text{cm}$.

In Figs. 9 and 10, the observed images of the InIm with a paraxial perfect lens array and an NIL array of the same effective focal length $f_{N,eff} = 0.2\text{cm}$ are presented, respectively. By

#101915 - $15.00 USD Received 23 Sep 2008; revised 22 Nov 2008; accepted 11 Dec 2008; published 17 Dec 2008

comparing the images for a real object observation in Fig. 8, it is clear that the synthesized 3D images of both the perfect paraxial lens array and the NIL array correctly express the views of the real object.

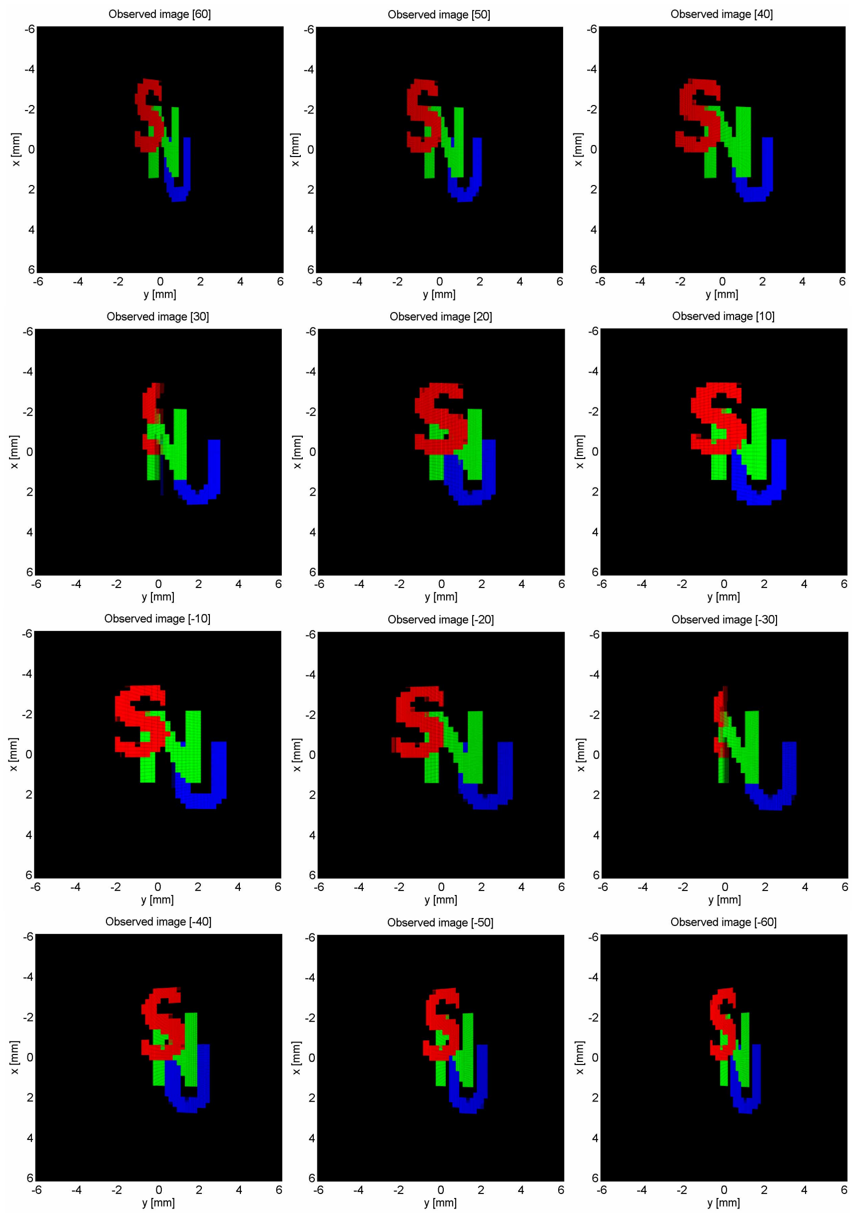

Fig. 11. Images of the InIm with a perfect paraxial lens array of focal length $f_{P,eff} = 1\text{cm}$.

In the case of the NIL array, the low brightness and pixelate 3D images are due to the finite effective window size, as explained in Fig. 5. The particularly low brightness of the $\pm 60(\text{deg.})$ images is mainly due to a slight elongation of the focal length. In spite of the low brightness, the synthesized images are well matched to the observation images for the real object at those viewing angles.

#101915 - $15.00 USD Received 23 Sep 2008; revised 22 Nov 2008; accepted 11 Dec 2008; published 17 Dec 2008

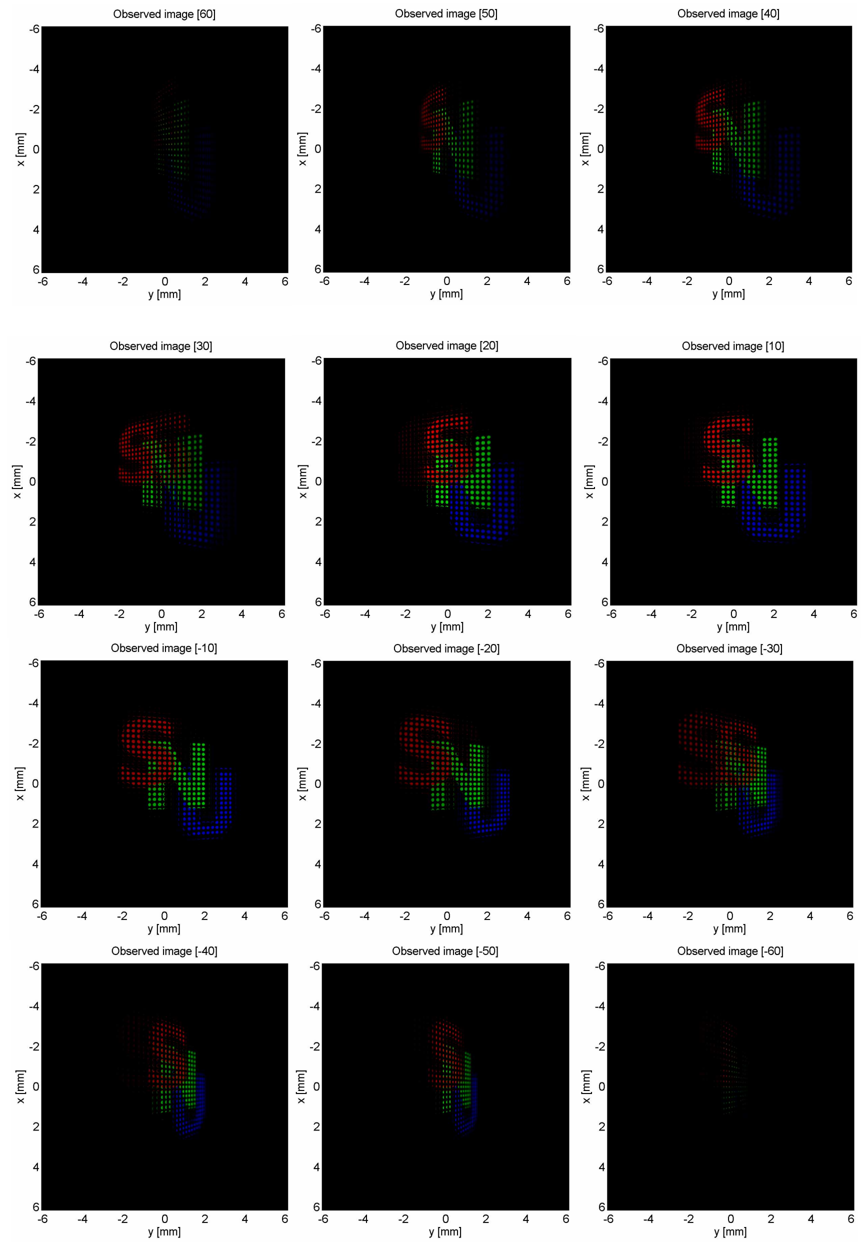

Fig. 12. Images of the InIm with a PIL array of effective focal length $f_{P,eff} = 1\text{cm}$.

In Figs. 11 and 12, observed images for the InIm with a paraxial perfect lens array and a PIL array of the same effective focal length $f_{P,eff} = 1\text{cm}$ are presented, respectively. In Fig. 11, the flipping effect due to the limited angular bandwidth of the elemental image can be clearly observed in the $\pm 30(\text{deg.})$ images. However, in the range of the viewing angles less than $\pm 30(\text{deg.})$, the observed images are quite similar to the observed images of the real object.

#101915 - $15.00 USD Received 23 Sep 2008; revised 22 Nov 2008; accepted 11 Dec 2008; published 17 Dec 2008

For viewing angles larger than $\pm 30(\mathrm{deg.})$, it can be seen that the observed image does not express the correct 3D images, in comparison with images of the real object. This incorrectness can be ascribed to a lack of image recording angular bandwidth due to the short lens focal length of the lens. The images observed at $\pm 60(\mathrm{deg.}) \sim \pm 40(\mathrm{deg.})$ show no distinct parallax. This effect equally appears in the InIm with the PIL array, as shown in Fig. 12. In the PIL InIm, additional image distortions are observed in the case of images at $\pm 60(\mathrm{deg.}) \sim \pm 40(\mathrm{deg.})$, which is due to the focal length elongation, as indicated in Fig. 5(c). Therefore the limitation in the viewing angle for PIL within about $\pm 30(\mathrm{deg.})$ is manifested in this simulation.

Let us compare the image quality of the PIL and NIL InIm systems. Comparing Figs. 13(a) and 13(b), it can be seen that the overall brightness of the NIL system is lower than that of the PIL system. We can say that the origin of the overall low brightness of the NIL system observed in the simulation can be attributed to the relative lack of the focusing accuracy for NIL with respect to the requirement for a high resolution in the elemental image and the method used in its synthesis. Actually, as analyzed in Fig. 4, the level of aberration for PIL is no less than for NIL. However, at the same aberration level, the shorter focal length lens feels a relative lack of focusing accuracy, compared to the longer focal length lens, since an element in the elemental image synthesized by an aberration free perfect paraxial lens system is smaller for a shorter focal length lens than for a longer focal length lens, thus the short focal length lens system requires a much higher resolution elemental image and each image element size is reduced.

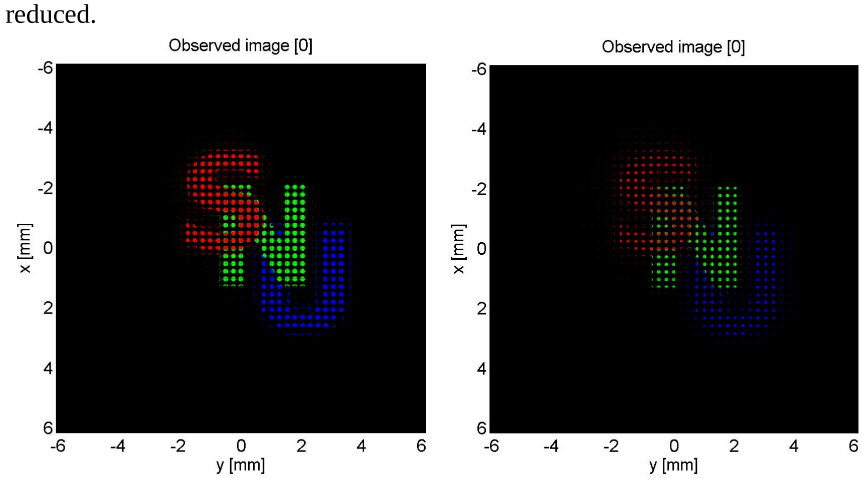

(a) (b)

Fig. 13. Comparison of InIm images with (a) PIL array and (b)NIL array.

Since the focal length for NIL is much smaller than that for PIL, each image element area in the elemental image for the NIL system is smaller than that for the PIL system, so the dark area in the elemental image for the NIL system is much larger than that for the PIL system. This is vividly shown in Fig 7. Therefore, although the NIL and PIL systems have a similar aberration level, since the resolution level required for the NIL system is much higher than that for PIL, an observer of the present NIL system sees a low brightness image which originates from the lack of the focusing accuracy associated with NIL with respect to the tight requirement for a high resolution elemental image. This lower brightness is inevitable in the NIL system described herein. The aberration associated with the present NIL needs to reduced further to improve the image brightness.

Regarding material loss associated with practical negative index metamaterials [24, 25], it should be noted that NIL is considerably thinner than the PIL as indicated in Fig. 1. In

#101915 - $15.00 USD Received 23 Sep 2008; revised 22 Nov 2008; accepted 11 Dec 2008; published 17 Dec 2008

practice, the material loss associated with NIL can be serious, but the lens thickness required for effective focusing is small, which is an advantageous property, in terms of compensating for material loss for NIL. Transmission loss in NIL is a function of the viewing angle, since the optical path length inside the NIL varies with the incidence angle. As the viewing angle increases, the optical path length inside the NIL becomes longer. However, the NIL lens can have a relatively thin lens thickness. In the paraxial regime, the consideration of the loss variation for the viewing angle can be mitigated.

In addition, we wish to comment on an important physical feature of the negative index meta-materials, i.e. dispersion. We conjecture that all color (red, green, blue; RGB) imaging is possible within the framework as an NIL InIm system with high dispersion property if a specially designed dispersion compensated multiple-lens-group is used for the lens array. In the case of InIm, the most serious problem induced by chromatic dispersion is the variation in the focal length of the lens array as a function of wavelength. In the example system described in this paper, the distance between the image panel and the lens array is set to the focal length of the elemental lens. Defocusing due to chromatic dispersion produces image blurring, cross-talk and image mixing between two adjacent views. Thus, the basic and important constraint for full color InIm imaging is a robust focal length.

In practice, to realize full color imaging, the lens array should be designed through advanced dispersion compensating techniques. This topic is beyond the scope of this paper. In this paper, the lens used in the study is assumed to have no chromatic dispersion properties, thus the color-imaging simulation presented in this paper can be considered to be dispersion compensated InIm imaging for the sake of simplicity and convenience. In addition, the simulation results can be seen as a single color image with just color indication (RGB) of three different depth objects, S, N, U for clear visualization. In our future work, we plan to report on chromatic dispersion compensation of negative refractive index meta-material lens with emphasis on physical parameters.

4. Conclusion

In this paper, we report on an investigation of the 3D imaging properties of an unusual high viewing angle $-60(\deg.) \sim +60(\deg.)$, negative index plasnoconcave lens array. We performed a comparative quantitative study of the limitations of a practical positive index planoconvex lens array in the respective cases of a perfect lens and a spherical lens having the same effective focal lengths. The virtual realization of the very short focal length spherical singlet using a negative index lens was devised. Although the negative index lens is a technology for use in the distant future, theoretical studies of wide viewing angle InIm are feasible and reasonable with a virtual setup with a negative lens array. Several imaging properties that are necessary in 3D InIm such as focusing property, aberration, and effective transmission window, as well as Fourier transform properties, were analyzed for both a negative index planoconcave lens and a positive index planoconvex lens. The negative index lens can have a very short focal length $f_{N,eff} = 0.4R$ that can not be even theoretically realized by the positive lens, $f_{P,eff} = 2R$. The limited effective transmission window size is problematic for both negative and positive lenses. As a result, the low brightness of 3D images at viewing angles larger than $\pm 60(\deg.)$ can be expected and should be further studies, in an attempt to overcome problems associated with transmission efficiency.

Acknowledgment

The authors acknowledge the support of the Ministry of Education, Science and Technology of Korea and the Korea Science and Engineering Foundation through the Creative Research Initiative Program (Active Plasmonics Application Systems).

#101915 - $15.00 USD Received 23 Sep 2008; revised 22 Nov 2008; accepted 11 Dec 2008; published 17 Dec 2008